Antarctic sea ice parameters from AMSR-E data using two techniques and comparisons with sea ice from SSM/I

Claire L. Parkinson[1] and Josefino C. Comiso[1]

Received 30 March 2007; revised 15 October 2007; accepted 30 November 2007; published 16 February 2008.

[1] Antarctic sea ice concentrations and extents, derived from the satellite passive microwave data of the Advanced Microwave Scanning Radiometer for the Earth Observing System (AMSR-E) are close but not identical depending on which of two major algorithms is used in the calculations. Overall, ice extents tend to be higher and ice concentrations lower when determined from the AMSR-E bootstrap algorithm (ABA) than when determined from the enhanced NASA team (NT2) algorithm, although the differences are within the algorithm error bars. Both algorithms obtain similar negative slopes for the lines of linear least squares fit through the short (4.5-year) AMSR-E data record available so far. When the ABA results are compared with results from the bootstrap algorithm applied over the same time period to data from the Special Sensor Microwave Imager (SSM/I), the two bootstrap results, from different satellites and different instruments, match even more closely than the ABA versus NT2 results from the same AMSR-E instrument. This is encouraging and is likely due to considerable effort to minimize the AMSR-E versus SSM/I bootstrap differences, in consideration of extending the SSM/I record (which goes back to 1987) with the AMSR-E results.

Citation: Parkinson, C. L., and J. C. Comiso (2008), Antarctic sea ice parameters from AMSR-E data using two techniques and comparisons with sea ice from SSM/I, *J. Geophys. Res.*, *113*, C02S06, doi:10.1029/2007JC004253.

1. Introduction

[2] On 4 May 2002, NASA's Aqua spacecraft was launched from Vandenberg Air Force Base carrying the Japanese Advanced Microwave Scanning Radiometer for the Earth Observing System (EOS) (AMSR-E) and five other Earth-observing instruments [*Parkinson*, 2003]. AMSR-E provides finer spatial resolution than earlier satellite passive microwave instruments through its large main reflector and provides an additional improvement over all other current satellite passive microwave instruments through its wider range of microwave frequencies [*Kawanishi et al.*, 2003]. One of the many variables being examined with AMSR-E data is polar sea ice, important for the large area it covers, the insulation it provides between the ocean and atmosphere, its reflection of solar radiation, and a range of additional impacts it has on polar climates and ecosystems [e.g., *Parkinson*, 2004].

[3] Sea ice concentrations (percent areal coverages of ice) have been calculated from the AMSR-E data through two major sea ice algorithms: an enhanced NASA team algorithm (NT2) and the AMSR-E bootstrap algorithm (ABA), both of which are described by *Comiso et al.* [2003]. Sea ice concentrations also continue to be calculated from data from the Special Sensor Microwave Imager (SSM/I) on board satellites of the Defense Meteorological Satellite Program (DMSP), and although the SSM/I data have a coarser spatial resolution than the AMSR-E data, they have tremendous value, because the SSM/I record extends back to 1987 and has been merged with 1978–1987 data from the Scanning Multichannel Microwave Radiometer (SMMR) on board NASA's Nimbus 7 satellite to provide a decades-long sea ice data record [e.g., *Bjorgo et al.*, 1997; *Cavalieri et al.*, 1999; *Parkinson et al.*, 1999; *Zwally et al.*, 2002]. As with other data products derived from satellite data, the existence of more than one algorithm to derive sea ice concentrations can be both frustrating and valuable. It can be frustrating for potential users of the data who are not interested in the technique but simply want a high-quality data set to use in modeling or other efforts; but it can be valuable in terms of providing insights into the proper interpretation of the satellite signal, through analyses of the causes of the differences where the algorithms produce different results. No algorithm will provide a perfect representation of reality. The purpose of this paper is to provide quantitative comparisons between the Southern Ocean sea ice results obtained from the two AMSR-E algorithms and between the AMSR-E and SSM/I results from the bootstrap algorithm. A companion paper by *Comiso and Parkinson* [2008] examines the Arctic results.

2. Data, Algorithms, and the Antarctic Setting

[4] Collection of high-quality AMSR-E data began on 18 June 2002, and has continued for most days at least

[1]Cryospheric Sciences Branch, NASA Goddard Space Flight Center, Greenbelt, Maryland, USA.

This paper is not subject to U.S. copyright.
Published in 2008 by the American Geophysical Union.

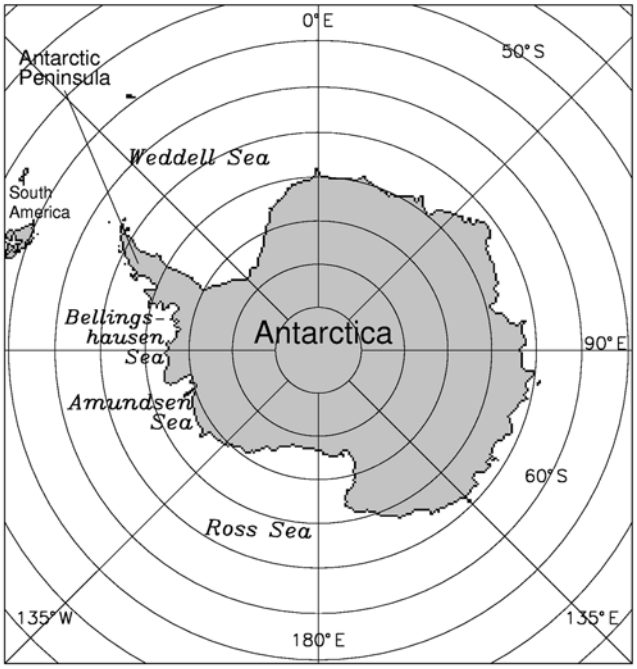

Figure 1. Location map.

through early 2008. SSM/I data have also been collected on most days over the same period, as well as on most days for the preceding 14 years. Among the most used algorithms for generating sea ice concentrations from these data sets are: (1) an algorithm based on polarization and gradient ratios originally developed in the 1980s for the Nimbus 7 SMMR data and termed the NASA team (NT) algorithm [*Cavalieri et al.*, 1984; *Gloersen et al.*, 1992], then upgraded to an enhanced NASA team, or NT2, algorithm [*Markus and Cavalieri*, 2000] and revised further for use with the AMSR-E data [*Comiso et al.*, 2003], and (2) an algorithm based on cluster analysis and termed the bootstrap algorithm, also originally developed in the 1980s for use with the Nimbus 7 SMMR data [*Comiso et al.*, 1997] and also upgraded since then [*Comiso et al.*, 2003], to an AMSR-E bootstrap algorithm, abbreviated ABA. Relevant aspects of the ABA and the NT2 algorithms are described in the companion paper for the Arctic [*Comiso and Parkinson*, 2008].

[5] In the case of the SSM/I data, the results presented here are from version 3 of the SSM/I bootstrap algorithm (abbreviated SBA). SBA is the latest version of the SSM/I bootstrap algorithm, adjusted to minimize the differences between the SBA and ABA sea ice concentrations, as described in more detail in the companion paper [*Comiso and Parkinson*, 2008]. The NT algorithm, for SMMR and SSM/I data, and the NT2 algorithm, for AMSR-E data, are compared in the work by *Markus and Cavalieri* [2000].

[6] An important consideration when comparing results from the two algorithms is the environmental setting. In marked contrast with the Arctic situation, where much of the sea ice cover is hindered from equatorward expansion by the Eurasian and North American continents, in the Antarctic the sea ice cover does not have a confining equatorward boundary and hence can expand as far north as dynamics and thermodynamics allow. At the Southern Ocean ice edge, new ice is continually growing in winter, initially as frazil ice that grows into pancake ice of different sizes and thicknesses. Because of waves and wind, the ice cover is generally loose and mobile around the edge. Waves are significantly attenuated, however, inside an ice pack, and the interior of the Antarctic ice cover is typically quite consolidated, a condition generally reached within tens of kilometers of the ice edge. Another major environmental consideration affecting the Antarctic ice cover is that it surrounds the Antarctic continent, which reaches elevations exceeding 3000 m and greatly affects the atmospheric flow in the vicinity. Cold and intense katabatic winds from the continent are frequent along the coastal areas and often locally drive the sea ice cover to the north, away from the continent, thereby creating polynyas (regions of open water within an ice cover) along the coast [*Bromwich and Kurtz*, 1984]. These polynyas have been regarded as ice factories, since the regions are sites of high rates of ice production as the newly formed ice is driven northward, exposing more surface water, which quickly freezes in the very cold environment [*Markus et al.*, 1998]. The Antarctic ice cover, unconfined by continents to the north, is also very dynamic, driven in part by the Antarctic circumpolar current [*Olbers et al.*, 2004] as well as by the wind patterns. The oceanic and atmospheric forcing leads to large-scale clockwise gyres in the ice cover, such as the Weddell gyre and the Ross Sea gyre. These patterns are associated with strong winds that generally cause divergence and breakup in the ice cover, enhanced also by tidal forcing and causing widening leads. Still, the interior pack ice usually remains highly concentrated because the leads generally become ice covered within a few hours of their formation, as new ice forms in them.

[7] Because the Antarctic continent covers the central south polar region, the Antarctic sea ice cover, to the north of the continent and hence at lower latitudes, does not have the substantial area of multiyear ice that exists in the Arctic. Also, because the Antarctic ice can freely expand equatorward (and the winds are not generally pushing the ice toward the continent), while much of the Arctic ice is confined by land boundaries to the south, the Antarctic ice tends to have less ridging than the Arctic ice. Another contrast is the lesser amount of meltponding in the Antarctic. The smaller amount of multiyear ice, ridging, and meltponding all help to simplify the interpretation of the satellite signal for the Antarctic ice; but a different factor that instead adds complications is the issue of ice flooding. In the Antarctic, perhaps more so than in the Arctic although the data are not sufficient to determine that, snow cover sometimes depresses the ice surface below the waterline, flooding the snow and thereby adding a water emission to the signal received by the satellite.

[8] The abundance of new ice of different stages of development throughout the Antarctic ice pack also complicates the retrieval of sea ice concentrations. Affected by thickness, salinity, ice surface roughness, and snow cover, the emissivity of new ice is highly variable, as well as being dependent on the frequency of the measured radiation. The AMSR-E channels used in the sea ice derivations from the ABA algorithm are the vertically polarized 18.7 GHz frequency (1.6 cm wavelength) channel and the vertically and horizontally polarized 36.5 GHz (0.8 cm wavelength)

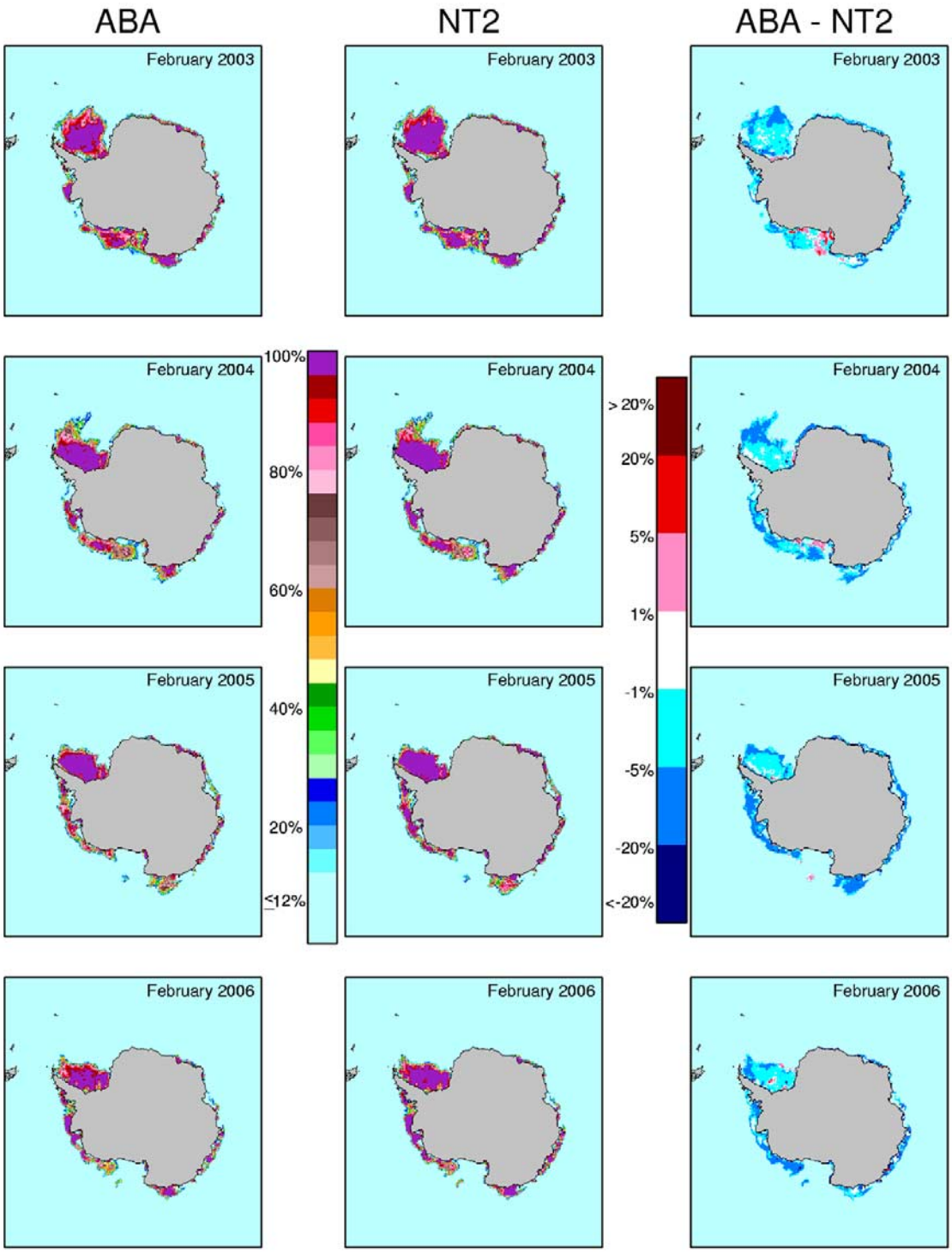

Figure 2. February monthly average Southern Ocean sea ice concentrations as derived from the AMSR-E data using the AMSR-E bootstrap (ABA) and enhanced NASA team (NT2) algorithms, along with their differences (ABA–NT2) for each year 2003–2006.

channels. The NT2 algorithm uses the vertically and horizontally polarized 18.7 GHz channels, the vertically polarized 36.5 GHz channel, and the vertically polarized 89 GHz (0.34 cm wavelength) channel. The 89 GHz channel is used in order to adjust for the variability of the polarization ratio at 18.7 GHz (a ratio used in the NT2 calculations) due to layering in the ice cover [*Markus and Cavalieri*, 2000]. The use of the 89 GHz channel introduces an added complication because of the higher sensitivity of the 89 GHz data than the 18.7 GHz or 36.5 GHz data to atmospheric effects and snow cover, a complication that is partly alleviated in the NT2 technique through the use of a radiative transfer

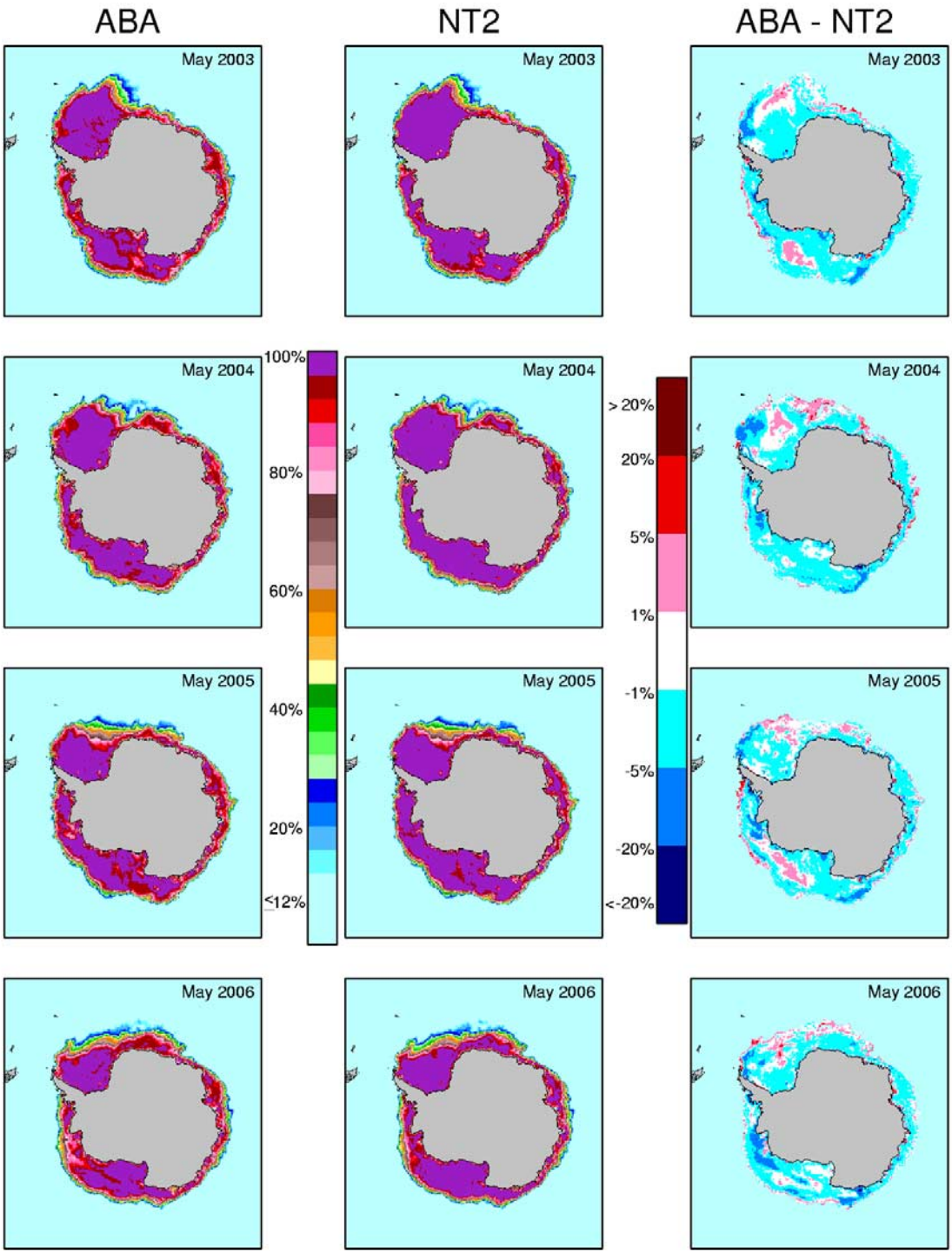

Figure 3. Same as Figure 2 but for May.

calculation for the atmosphere. The different channels also have different sensitivities to ice thickness and surface conditions, especially in new ice regions. Particularly important, the ice emissivity at 89 GHz increases faster with ice thickness (for very thin ice) than does the emissivity at 18.7 and 36.5 GHz, so that in new ice regions, with very thin but growing ice, the ice concentrations derived by NT2, incorporating the 89 GHz data, tend to be higher than those derived by ABA. This is an advantage in using the NT2 algorithm, as it is able to recognize the presence of the very thin ice, obtaining more accurate ice concentrations in new ice regions. An advantage of the ABA algorithm is its use exclusively of channels that are less sensitive than the 89 GHz channel to atmospheric and surface effects that can create faulty ice concentration results. In section 3.1, we examine how such contrasts are reflected in the derived geophysical parameters.

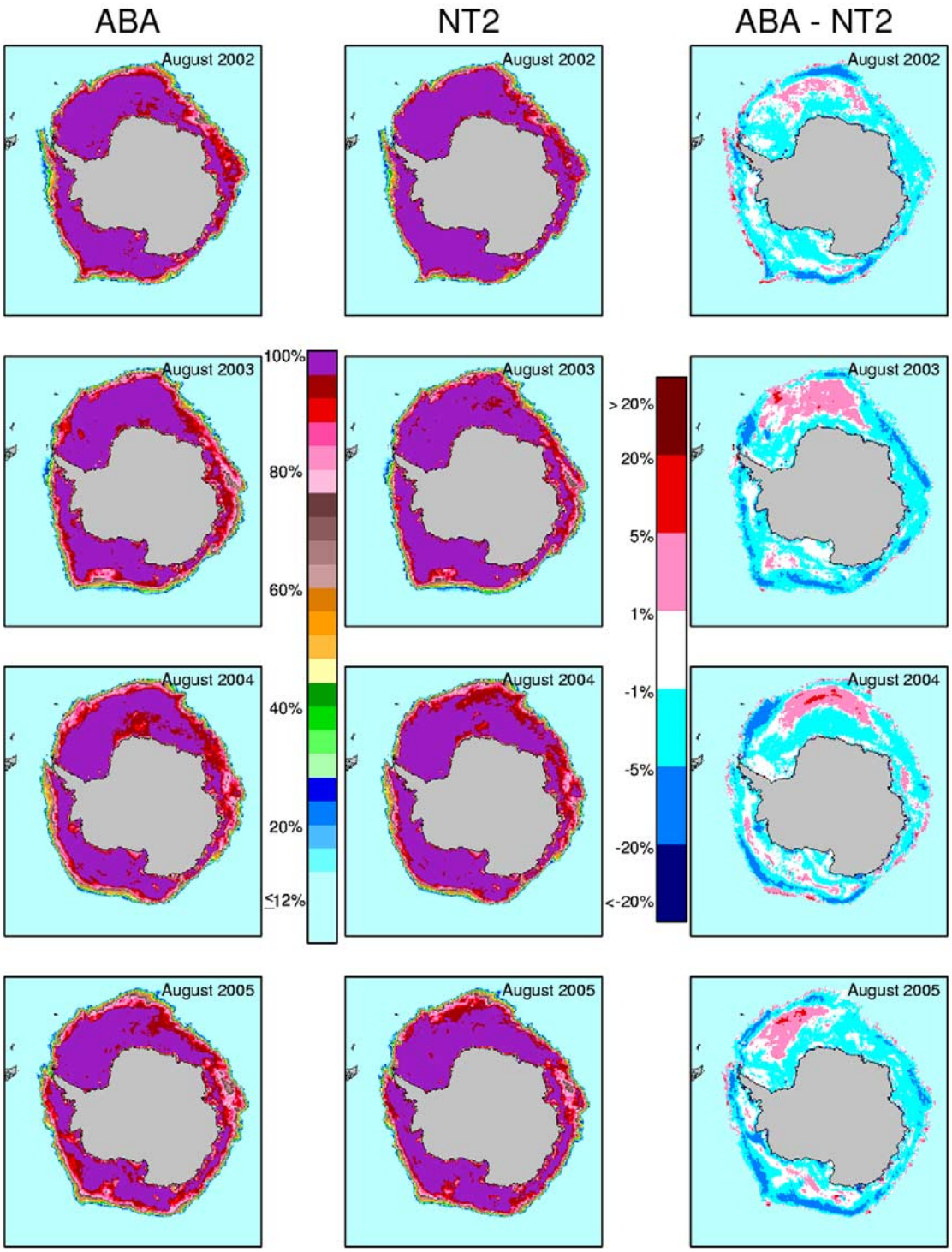

Figure 4. Same as Figure 2 but for August 2002–2005.

[9] Weather conditions can affect the radiative signal, sometimes showing false indications of sea ice in the open ocean. By mapping ice only where ice is calculated to cover at least 12% of the pixel and by accumulating ice extents and areas only where ice covers at least 15% of the pixel, many of the spurious indications of ice are eliminated, and these 12% and 15% ice cutoffs are done consistently for both algorithms. Both algorithms, however, also incorporate additional weather filters to eliminate or at least greatly reduce the remaining false indications of sea ice. For the AMSR-E data, the NT2 algorithm employs a pair of weather filters based on threshold values for the gradient ratios between the 36.5 GHz and 18.7 GHz data and between the 23.8 and 18.7 GHz data, whereas the bootstrap algorithm employs a weather filter based on the brightness temper-

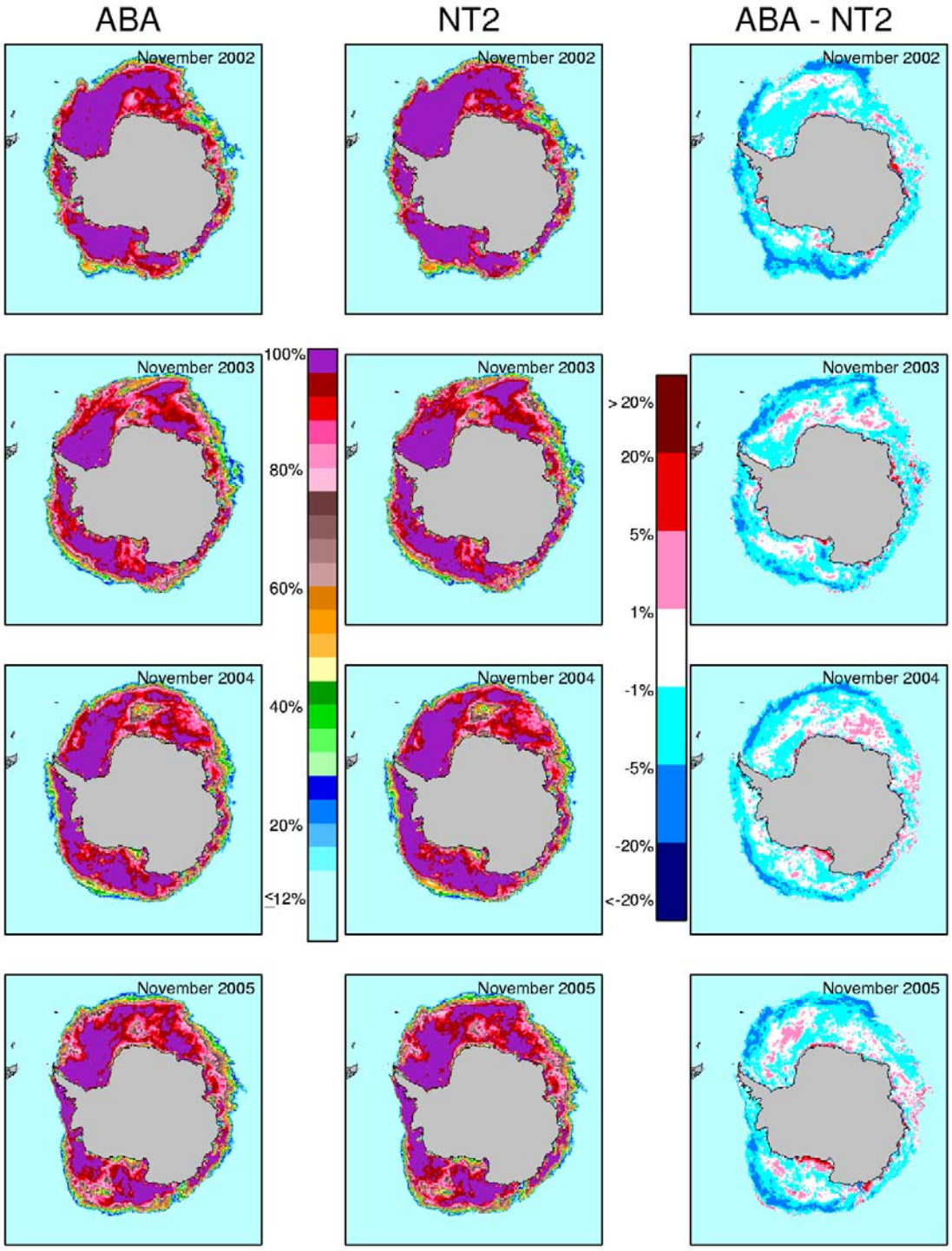

Figure 5. Same as Figure 2 but for November 2002–2005.

ature difference between the 23.8 and 18.7 GHz data. More details on the weather filters and other aspects of the data handling can be found in work by *Comiso et al.* [2003] and *Comiso and Parkinson* [2008].

[10] The instantaneous fields of view (ground footprints) of the relevant AMSR-E channels are as follows: 27 km × 16 km for the 18.7 GHz channels, 31 km × 18 km for the 23.8 GHz channels, 14 km × 8 km for the 36.5 GHz channels, and 6 km × 4 km for the 89 GHz channels. The corresponding values for the SSM/I are: 69 km × 43 km for the 19.35 GHz channels, 60 km × 40 km for the 22.235 GHz channels, 37 km × 28 km for the 37 GHz channels, and 15 km × 13 km for the 85.5 GHz channels. In line with the finer spatial resolution of the data from the AMSR-E, the AMSR-E sea ice data records are provided at gridded spatial resolutions of 12.5 km and 25 km, while the SSM/I data records are provided only at the gridded spatial resolution of 25 km. Both the AMSR-E and the SSM/I obtain full data

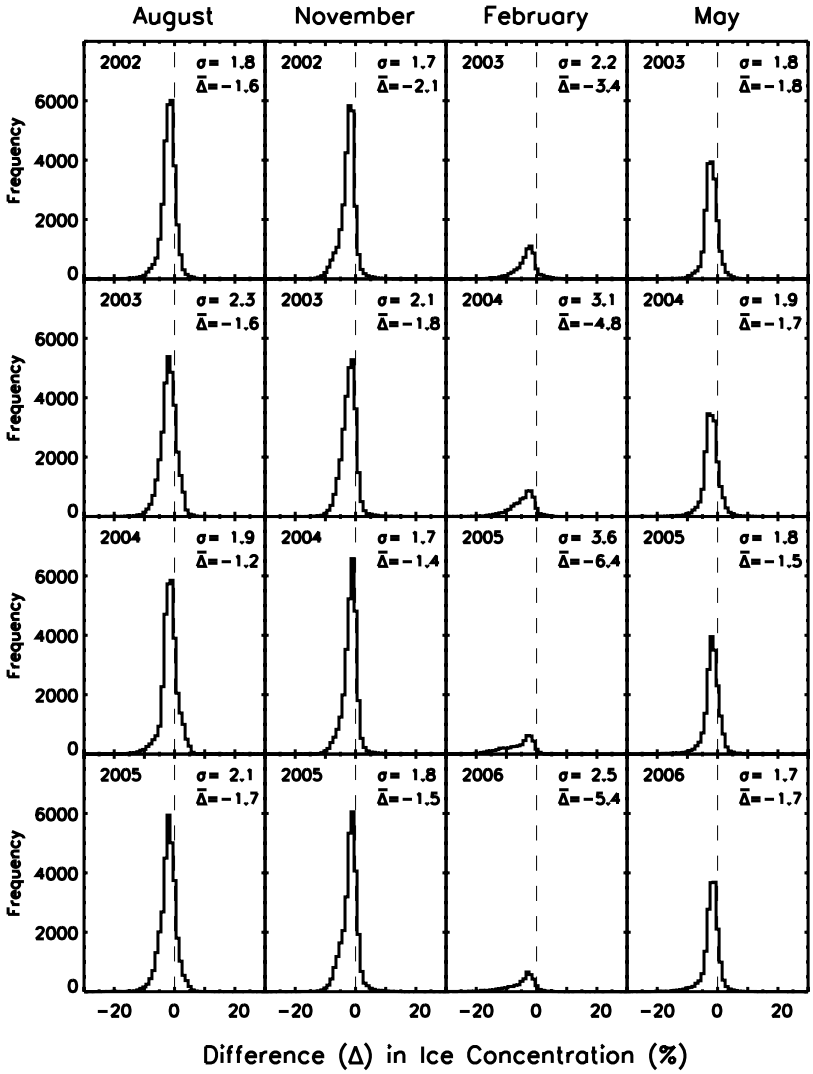

Figure 6. Histograms of the differences (ABA−NT2) between monthly averaged sea ice concentrations derived from the AMSR-E data using the ABA and NT2 algorithms. The histograms incorporate the data from each data point (pixel) of the difference maps in Figures 2–5. The standard deviation (σ) of a Gaussian fit to the data and the average of the ice concentration differences (Δ) for each plot are shown in the top right corner of each plot.

coverage of the Southern Ocean. The AMSR-E, SMMR, and SSM/I data products are all available at the U. S. National Snow and Ice Data Center (NSIDC) in Boulder, Colorado.

3. Results

3.1. AMSR-E Bootstrap Versus NT2 Algorithm Comparisons

3.1.1. Antarctic Sea Ice Concentrations

[11] In the Southern Ocean (Figure 1), sea ice coverage undergoes a quite significant seasonal cycle, typically reaching a minimum ice extent of less than 4×10^6 km^2 in February of each year and a maximum ice extent exceeding 17×10^6 km^2 in August or September, with occasional maxima as late as October [e.g., *Gloersen et al.*, 1992]. Here we use the months of February, May, August, and November (representing the four seasons) to illustrate the spatial distributions of the ice concentrations derived from the AMSR-E data using the ABA and NT2 algorithms, with the mapped differences (ABA−NT2) between the two results also presented (Figures 2, 3, 4, and 5). For each month, the figures present the maps for the first 4 years of the AMSR-E results, i.e., 2003–2006 for February and May, and 2002–2005 for August and November.

[12] The ice concentration maps (Figures 2–5) show that both of the algorithms obtain very close to the same geographic picture of sea ice coverage each month, with the same major interannual differences. For instance, in the February images both algorithms reveal a full-scale open water polynya off the southeastern coast of the Antarctic Peninsula in 2003 but not in any of the other 3 years, and similarly, in each year the two algorithms reveal the same pattern of polynyas and the same pattern of ice coverage around the continent, even to the point of having the same islands of ice visible in the Ross Sea in February 2005 and, separately, in February 2006 (Figure 2). They also both

Table 1. Pixel Numbers for Figures 2–5

Month	Numbers of Pixels			Percent With > 20% Difference
	With Ice	ABA-NT2 ≥ 20%	ABA-NT2 ≤ −20%	
Feb 2003	6849	13	106	1.7
Feb 2004	6606	15	138	2.3
Feb 2005	5253	12	193	3.9
Feb 2006	4607	9	173	4.0
May 2003	19457	4	41	0.2
May 2004	18855	15	48	0.3
May 2005	18554	8	51	0.3
May 2006	17442	19	47	0.4
Aug 2002	29714	15	51	0.2
Aug 2003	30911	13	33	0.2
Aug 2004	30932	11	25	0.1
Aug 2005	31067	16	37	0.2
Nov 2002	27375	10	32	0.2
Nov 2003	28168	13	7	0.1
Nov 2004	28419	18	13	0.1
Nov 2005	28712	22	17	0.1

show a Ross Sea with a strong sequence of lessened February ice coverage from 2003 to 2004 to 2005, with a slight rebound in 2006, contrasting with a Bellingshausen Sea where the minimum February ice coverage occurred in 2004 (Figure 2). Despite the similarity of the images, the February difference maps show that although the ice concentrations calculated by the two algorithms generally differ by no more than 5%, in some localities they differ by more than 20% (Figure 2 and Table 1). A far greater area shows negative values (NT2 ice concentrations exceeding ABA ice concentrations) than positive values, although with some negative and some positive values occurring both internal to the pack and along the ice edge. The greater predominance of negative values can be explained by the higher sensitivity of the 89 GHz channels (versus the 37 GHz and lower frequency channels) to thin ice [*Comiso et al.*, 1989].

[13] As with the summer results (Figure 2), the results for the other three seasons (Figures 3–5) also show that the ABA and NT2 algorithms capture the same features of the ice cover, including the same polynyas and the same year-specific peculiarities of the ice edge. For instance, they both reveal a prominent arch of ice in the eastern Weddell Sea at about 0°E in May 2004 (Figure 3), they both reveal a prominent sharply pointed extension of ice northward from the eastern Ross Sea ice at about 145°W in August 2002 (Figure 4), and they both reveal a straight line extension of ice at about 85°E in November 2005 (Figure 5). As with the February results, the May, August, and November difference maps all reveal that the ice concentrations calculated by the two algorithms differ by amounts that in some localities exceed 20% but that typically are less than 5% (Figures 3–5 and Table 1). February stands out as the month with the largest percentage of the ice area having negative values, i.e., with the NT2 ice concentrations exceeding the ABA ice concentrations, and August stands out as the month having the largest percentage of the ice area having positive values, i.e., with the ABA ice concentrations exceeding the NT2 concentrations (Figures 2–5),

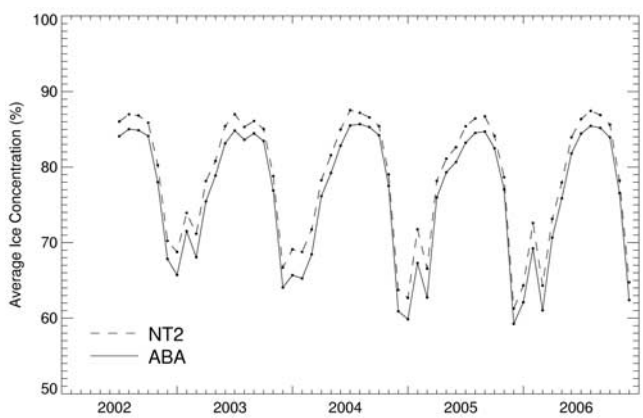

Figure 7. Average Southern Ocean ice concentrations, July 2002 to December 2006, as derived from the AMSR-E data using the NT2 and ABA algorithms. Each data point is obtained by spatially averaging over all pixels with >12% ice concentration in the corresponding monthly average ice concentration image (e.g., in the ice concentration images of Figures 2–5). Note that the 12% lower limit used here in the calculation of average ice concentrations differs from the 15% lower limit used in the calculations of ice extent and ice area. The reason for using 12% here is for consistency with the ice concentration color bars of Figures 2–5, i.e., so that the averaging for the plots is done over the full ice distribution depicted in Figures 2–5. (The major tick marks are at January of each year.)

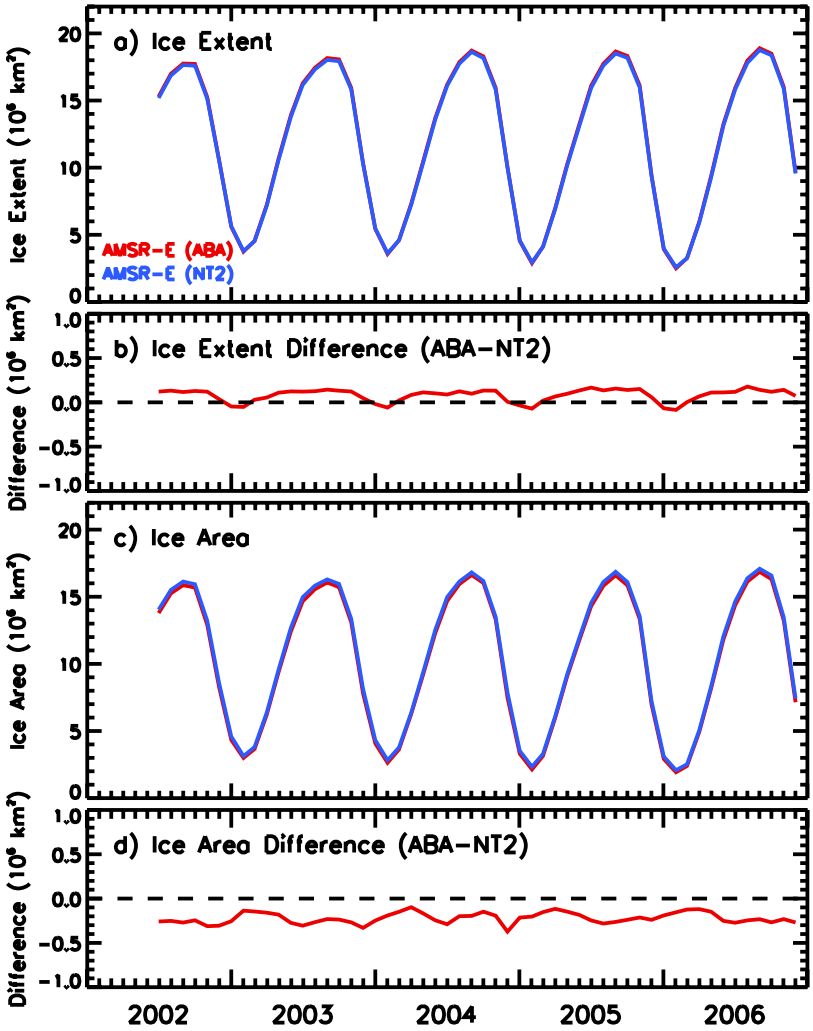

Figure 8. Monthly average Southern Ocean sea ice extents and areas from July 2002 to December 2006 as derived from the AMSR-E data using the ABA and NT2 algorithms: (a) sea ice extents, (b) ice extent differences between the ABA and NT2 results, (c) sea ice areas, and (d) ice area differences between the ABA and NT2 results.

although even in August there are more negative than positive values (Figure 4).

[14] The predominance of negative ice concentration differences (NT2 ice concentrations greater than ABA ice concentrations) is more explicitly quantified through histograms of the ice concentration differences (Figure 6). The histograms quantify the slight but prominent negative bias in each of the 16 months. Averaged monthly, the histogram peaks occur at −1.5%, −1.25%, −2.5%, and −2.0% ice concentration in August, November, February, and May, respectively, and the averages of the ice concentration differences are −1.53%, −1.7%, −5.0%, and −1.67% in August, November, February, and May. The bias is thus generally small considering that the errors in ice concentration have been estimated at about 5–10% for midpack winter conditions and higher for melt conditions near the ice edge. (Field campaigns for validation of the AMSR-E algorithms in the Antarctic were carried out in September 2003 and October 2004. The results from these campaigns have not yet been fully analyzed or published but should eventually provide more precise data on biases and errors.) The standard deviations for the data points incorporated in the plots of Figure 6, averaged by month, are ±2.9%, ±2.8%, ±6.1%, and ±3.1% for August, November, February, and May, respectively, in each case exceeding the standard deviations of the Gaussian fits, provided in Figure 6. By each measure, the bias and standard deviations are largest in February, in line with expectations because summer ice conditions are notoriously complex and nonuniform in both polar regions, with variable mixtures of rotting ice floes, meltponding, flooding, fresh snow, old snow, and other conditions. These varied conditions have different impacts on the surface emissivity for the different microwave channels.

[15] When averaged over the entire oceanic region with greater than 12% ice concentration, the monthly average ice concentrations derived from the AMSR-E data range between 59% and 88%, with a strong seasonal cycle showing the lowest ice concentrations in late spring and summer (December to March) and the highest ice concentrations centered in midwinter (Figure 7). The higher occurrence of negative versus positive values in the difference maps

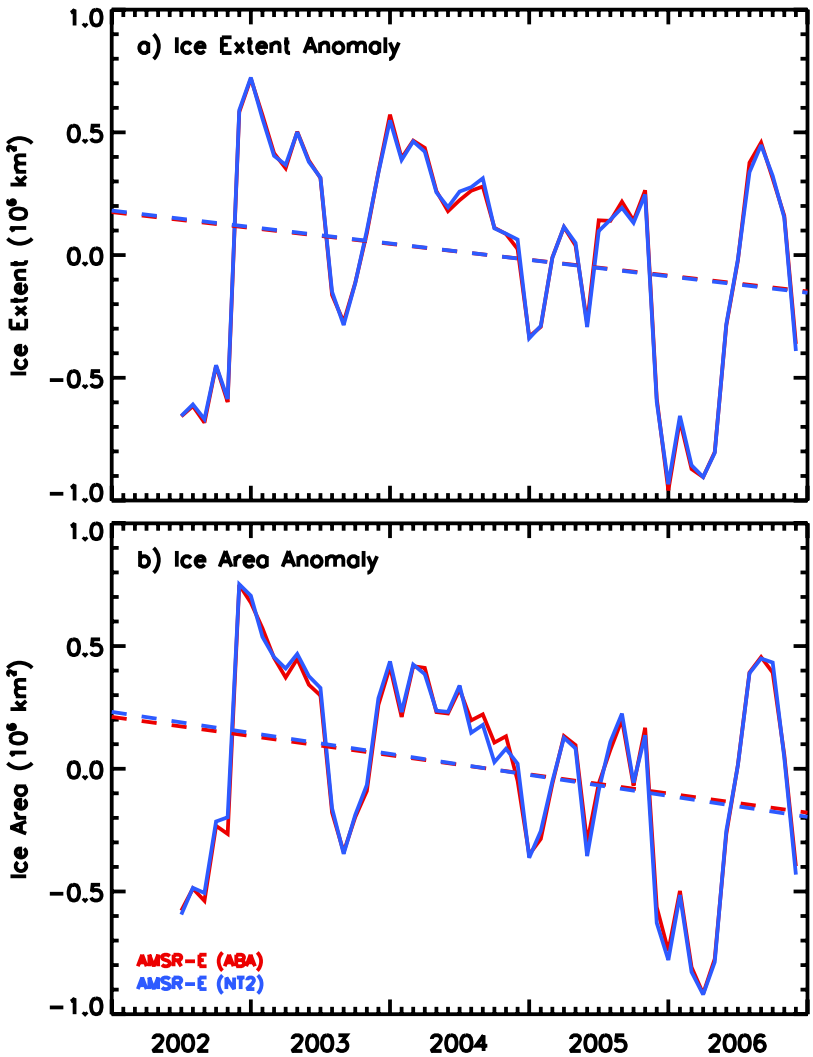

Figure 9. (a) Southern Ocean sea ice extent anomalies and (b) Southern Ocean sea ice area anomalies, calculated from the ice extents and ice areas displayed in Figure 8, i.e., from AMSR-E data using the ABA and NT2 algorithms.

(ABA−NT2) of Figures 2–5 shows up in Figure 7 with the NT2 average ice concentrations consistently higher than the ABA concentrations. The summertime average ice concentrations have a marked downward trend, although the wintertime average ice concentrations do not, a contrast that is consistent in both records (Figure 7). The two curves trend each other closely, including both having average ice concentration in February greater than in January or March in 2003, 2005, and 2006, and average ice concentrations in January 2004 greater than in the preceding and following months. The slight temporary rise in ice concentrations is especially explicable in February, as December and January generally have rapidly retreating ice covers and March a rapidly advancing ice cover, both circumstances that result in a large area of low monthly average ice concentrations.

3.1.2. Antarctic Sea Ice Extents, Areas, Anomalies, and Trends

[16] Sea ice "extent" is defined as the summed area of all ocean pixels having at least 15% sea ice concentration, integrated over the region of interest, which in our case is the entire Southern Ocean. Sea ice "area" is the summed areal coverage of ice, calculated as the sum of the product of ice concentration by pixel area, integrated over all pixels with ice concentration of at least 15%. Figure 8 presents the ice extent and ice area time series for both algorithms, over the period from the start of the AMSR-E monthly average record, July 2002, through the end of 2006, along with the difference plots. The ice extent curves from the two algorithms are close to identical, although the ABA obtains slightly higher ice extents in winter, spring, and autumn and slightly lower ice extents in summer than the NT2 algorithm (Figures 8a and 8b), as is apparent also from the maps of Figures 2 and 4, where the wintertime August maps show a predominance of positive values (ABA > NT2) around the ice edge (Figure 4) and the summertime February maps show a predominance of negative values (NT2 > ABA) around the ice edge (Figure 2). The ice area curves show more separation, with ice areas derived from the ABA being less than those derived from the NT2 algorithm throughout the year (Figures 8c and 8d), in line with the previously determined lower ice concentrations (Figure 7).

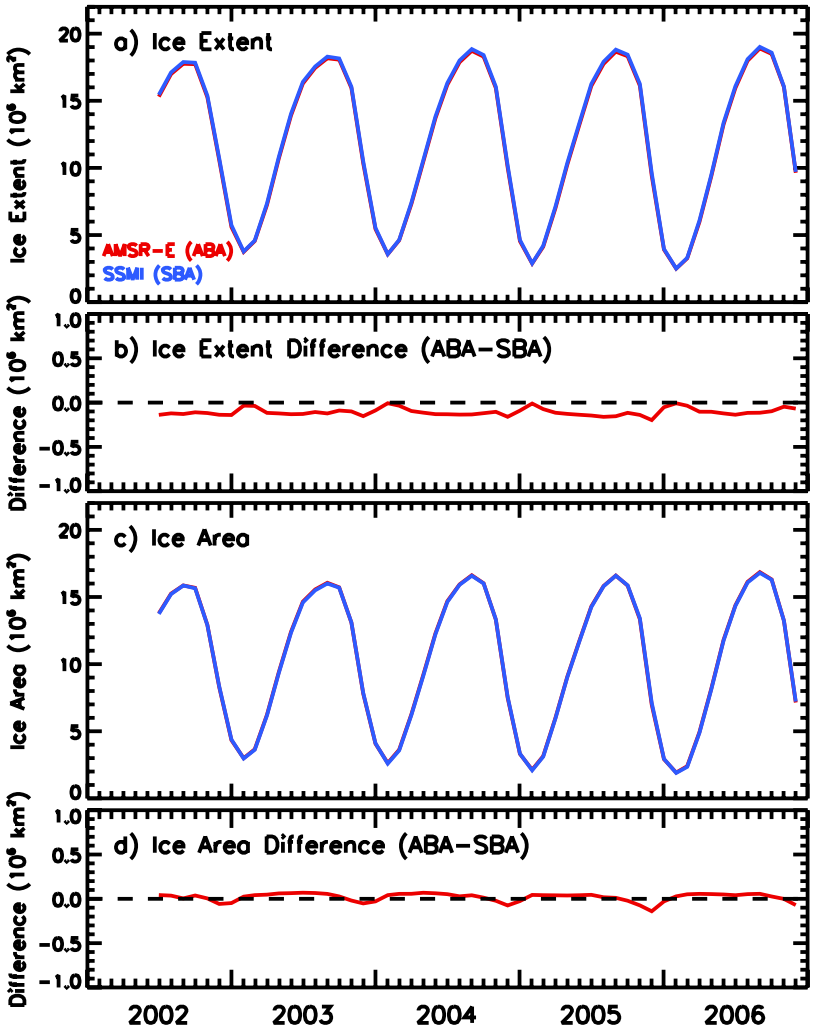

Figure 10. Monthly average Southern Ocean sea ice extents and areas from July 2002 to December 2006 as derived from the AMSR-E data and the SSM/I data using the bootstrap algorithm (ABA and SBA versions, respectively): (a) sea ice extents, (b) ice extent differences between the ABA and SBA results, (c) sea ice areas, and (d) ice area differences between the ABA and SBA results.

[17] Even when examined on a daily basis, the ice extents from the two algorithms are consistently well within 200,000 km^2 of each other (with the exception of a single outlier date), and the ABA–NT2 difference is consistently between −6.0% and +1.3% of the NT2 value (averaging −0.28%). The daily ice area values are consistently within 550,000 km^2 of each other, and the ABA–NT2 ice area difference is consistently between −11% and +0.3% of the NT2 value (averaging −2.95%).

[18] Although the AMSR-E record is far too short for meaningful climate trends, lines of least squares fit are calculated from the record in order to determine how much effect the differences in the ice concentrations derived from the two algorithms have on the trend results. To do this, time series of ice extent and ice area anomalies are calculated, in each case by taking the ice extent or area for the individual month and year and subtracting the average of the ice extents or areas for that month in each of the years throughout the data record (Figure 9). This procedure eliminates the seasonal cycle that dominates the ice extent and ice area curves of Figure 8. With the stretched vertical scales on the anomaly plots, both the ice extent and ice area anomaly curves show points of separation between the two plots (ABA and NT2). Still, the least squares trend lines are quite close for the ice extent anomalies (Figure 9a) and not far different for the ice area anomalies (Figure 9b). Ice extent trends, calculated as the slopes of the least squares fits, are −65,000 ± 46,000 km^2/a (−5.4 ± 3.8%/decade if the same trend were to continue for a full decade) for the ABA-derived results and −67,000 ± 45,000 km^2/a (−5.6 ± 3.8%/decade) for the NT2-derived results. Ice area trends are −78,000 ± 41,000 km^2/a (−7.5 ± 4.0%/decade) for the ABA-derived results and −86,000 ± 42,000 km^2/a (−8.1 ± 3.9%/decade) for the NT2-derived results. Although the ice area trends differ more than the ice extent trends, even with the ice area trends, the values derived from the two algorithms are each well within 1 standard deviation of the slope derived from the other algorithm.

3.2. AMSR-E Versus SSM/I Comparisons

[19] In this section we shift from comparing the sea ice results derived from the AMSR-E data using two different

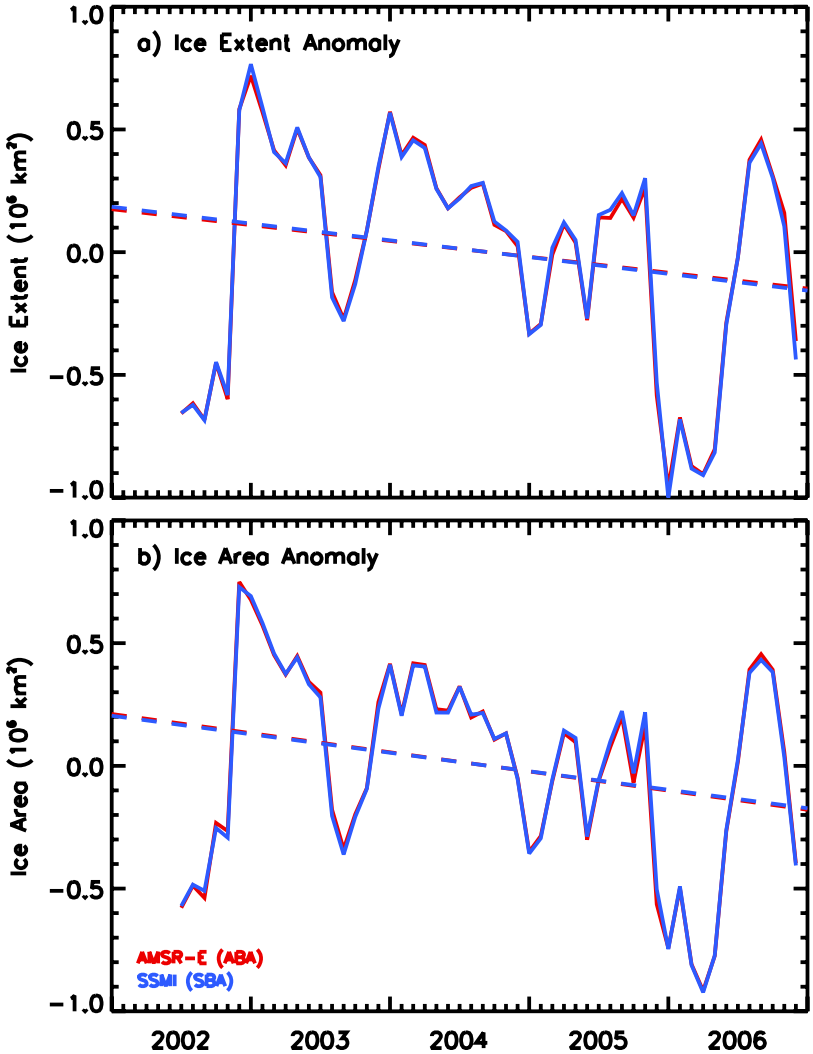

Figure 11. (a) Southern Ocean sea ice extent anomalies and (b) Southern Ocean sea ice area anomalies, calculated from the ice extents and ice areas displayed in Figure 10, i.e., from AMSR-E data and SSM/I data using the bootstrap algorithm's ABA and SBA versions.

algorithms to comparing the sea ice results derived from the AMSR-E and SSM/I data, both through use of the bootstrap algorithm (ABA for the AMSR-E data, SBA for the SSM/I data). Figure 10 presents the time series of ice extents and ice areas from the two instruments, along with the ice extent and ice area differences, and Figure 11 presents the corresponding anomalies. Results show a very good match between the bootstrap-derived values from both instruments. Ice extents are generally slightly higher from the SSM/I data (Figures 10a and 10b), while ice areas are generally slightly higher from the AMSR-E data except in late spring and early summer (Figures 10c and 10d). The extents, areas, and anomalies (Figures 10 and 11) overall match even more closely than the corresponding plots for the results from AMSR-E data as derived from the ABA and NT2 algorithms (Figures 8 and 9). The close correspondence between the ABA and SBA results is in part because the brightness temperatures from the AMSR-E and SSM/I have been intercalibrated and the algorithm tie points tuned for consistency. The resulting ABA and SBA ice concentrations from the two sensors are basically consistent within the pack, although some differences exist along the ice edge, the latter because of differences in sensor characteristics and especially the spatial resolution. The coarser resolution SSM/I sensor usually positions the ice edge further equatorward because of "smearing" and side lobe effects as discussed by *Comiso and Parkinson* [2008]. This phenomenon in turn causes higher estimates of ice extent with SSM/I than with AMSR-E data. Because the smeared ice edge has very low ice concentrations, the impact of this effect on the calculation of ice areas is noticeably less than its impact on the ice extents (Figure 10).

[20] The ice extent trend value calculated from the SSM/I data (i.e., the slope of the SBA line in Figure 11a) is −68,000 ± 46,000 km^2/a (−5.6 ± 3.8%/decade), which is about 5% greater in magnitude than the slope calculated from the AMSR-E data with the same basic algorithm (ABA slope in Figures 11a and 9a, i.e., −65,000 ± 46,000 km^2/a, or −5.4 ± 3.8%/decade, as presented earlier). The ice area trend from the SSM/I data (SBA slope in Figure 11b) is −75,000 ± 41,000 km^2/a (−7.3 ± 4.0%/decade), about 4% less in magnitude than the ABA trend.

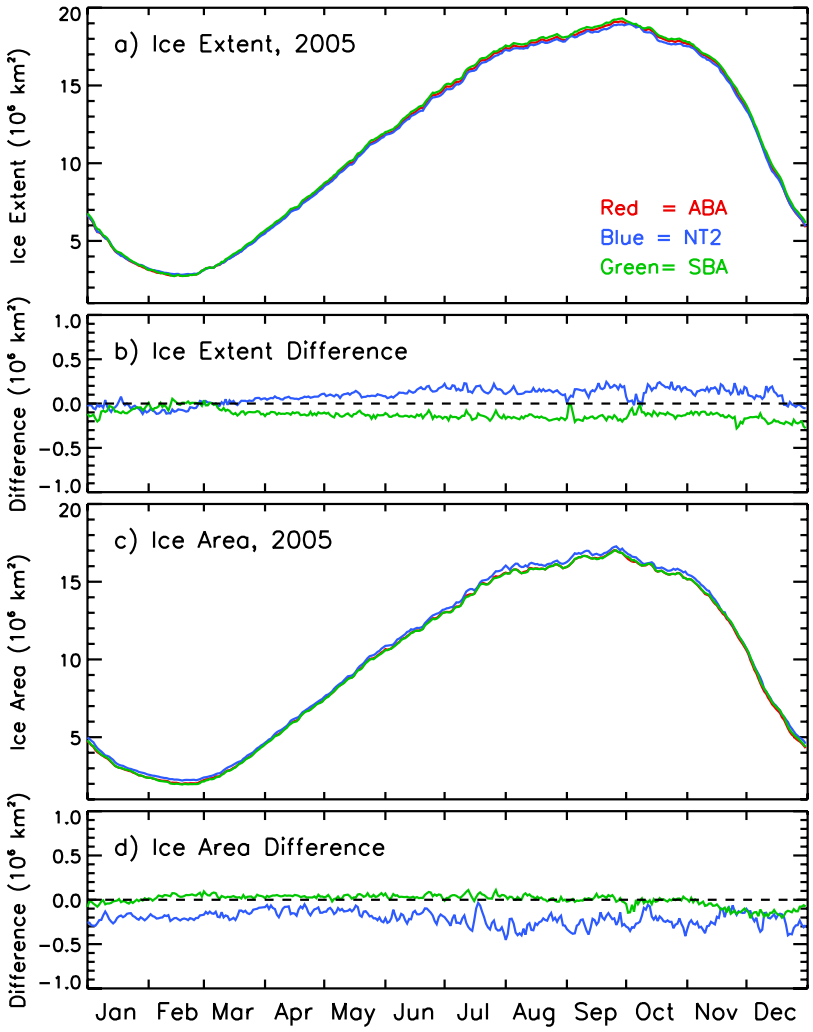

Figure 12. Daily Southern Ocean sea ice extents and areas in 2005 as derived from AMSR-E data with the bootstrap algorithm (ABA), AMSR-E data with the NT2 algorithm (NT2), and SSM/I data with the bootstrap algorithm (SBA): (a) sea ice extents, (b) ice extent differences for ABA–NT2 (blue) and for ABA–SBA (green), (c) sea ice areas, and (d) ice area differences for ABA–NT2 (blue) and for ABA–SBA (green).

[21] Figure 12 shows a year of daily ice extent and ice area values for all three sets of results, i.e., as derived from AMSR-E using the bootstrap algorithm (ABA), SSM/I using the bootstrap algorithm (SBA), and AMSR-E using the NT2 algorithm, thereby allowing examination of data derived from different sensors but the same algorithm (ABA and SBA) along with data derived from the same sensor but different algorithms (ABA and NT2). Also included in Figure 12 are the difference plots (Figures 12b and 12d). Although the 2005 ice extents are generally all within 4% of each other for the three methods, the NT2 results tend to have the lowest ice extents in all seasons except summer and the highest ice areas, and the SSM/I results tend to have the greatest ice extents and, for February through September, the lowest ice areas, just barely (Figure 12). These generalized results are valid for the other years of the record as well. As explained in the companion paper for the Arctic [*Comiso and Parkinson*, 2008], the coarser spatial resolution of the SSM/I data creates an equatorward smearing of the ice edge, helping to explain the higher SSM/I ice extent values.

[22] To examine further the possible impact of spatial resolution on ice extent and ice area results, a sensitivity study was performed on the impact of the ice edge location. Results are presented in Figure 13, where the time series of daily 2005 ice extents and ice areas derived from the AMSR-E data using the ABA algorithm are juxtaposed with the corresponding time series when the ice edge location is uniformly shifted equatorward by 6.25 km, 12.5 km, and 25.0 km, with all the additional ice, just outside the original ice edge, assumed to be at 15% ice concentration. The effect is understandably more pronounced on the ice extent curves, as the additional pixels have their full areas added to the ice extents (Figure 13a) but only 15% of their areas added to the ice areas (Figure 13b). Comparing Figures 12 and 13, the difference between the AMSR-E and SSM/I bootstrap results (ABA and SBA, Figure 12) are similar to the effect caused by a change in the location of the ice edge of somewhat less than 12.5 km (Figure 13). This is consistent with an explanation that the higher SBA values could be due to the coarser spatial

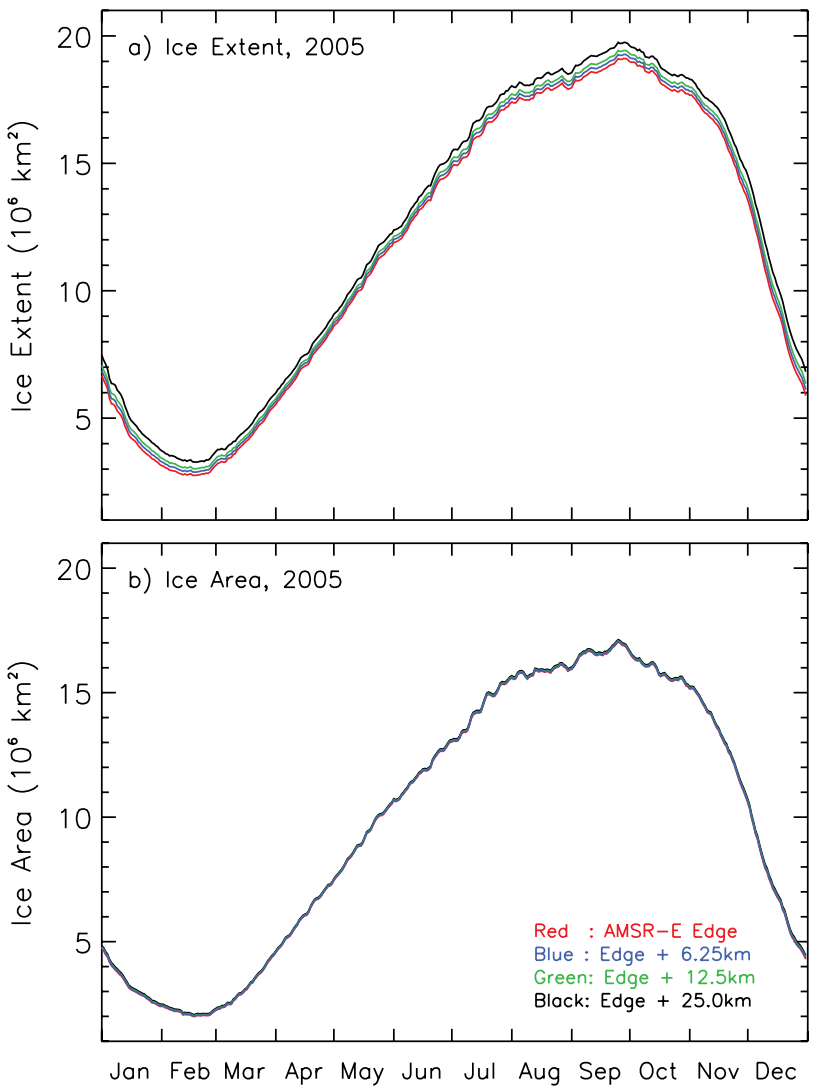

Figure 13. (a) Daily Southern Ocean sea ice extents and (b) daily Southern Ocean sea ice areas for the year 2005, as derived from AMSR-E data with the bootstrap algorithm (ABA, in red), plus the adjusted extents and areas calculated by extending the ice edge equatorward by 6.25, 12.5, and 25.0 km. For the ice area calculations, the additional ice pixels, beyond the AMSR-E-derived ice edge, are all assumed to have 15% ice concentration.

resolution of the SSM/I data and the resultant greater smearing of the ice edge.

4. Discussion

[23] Since the 2002 launch of the Aqua spacecraft carrying the AMSR-E sensor, the NT2 and ABA algorithms have both been used to derive sea ice concentrations and extents from the AMSR-E data, at times causing consternation for potential users of the data. The results presented here should provide some comfort that the two algorithms are obtaining derived ice amounts that are sufficiently close that for most purposes the choice of whether to use the ABA or NT2 results is not critical.

[24] Both the ABA and NT2 algorithms have a history extending back to the mid-1980s, as both are enhancements of algorithms developed originally for Nimbus 7 SMMR data and then modified for DMSP SSM/I data. The results from the earlier NASA team and bootstrap algorithms are compared by *Comiso et al.* [1997] for both hemispheres and all four seasons. Those results indicate that in the Antarctic the earlier bootstrap technique yielded ice concentrations generally higher than those from the earlier NASA team algorithm, sometimes by as much as 25%, while also yielding local areas with the team algorithm results higher than the bootstrap results by as much as 30%.

[25] The new results, with the enhanced NT2 and ABA algorithms, continue to show discrepancies, but the differences are much more modest, and, interestingly, are by and large in the opposite direction from the original team versus bootstrap contrasts, with the NT2 ice concentrations now generally higher than the ABA ice concentrations. This reversal is in part probably due to overshooting in the attempt to lessen the gap between the two sets of results. Further fine tuning of tie points with the revised algorithms could lead to an even closer NT2/ABA match. However, in view of the different techniques and different channels

used, fine tuning of tie points would not eliminate all differences. In particular, the use of the high-frequency 89 GHz channel in NT2 but not in ABA provides the NT2 calculations with the advantage of being more able to capture the presence of thin new ice, although at the same time produces the disadvantage of being more subject to contamination by atmospheric and snow cover effects. These factors will ensure some differences despite tie point adjustments.

[26] The match between the AMSR-E and SSM/I results from the bootstrap algorithm (ABA and SBA, respectively) is, in general, closer than the match between the bootstrap and NT2 results from AMSR-E. This is to some extent because of significant attention having been paid in previous efforts to ensure that the SSM/I bootstrap results could be extended with the AMSR-E bootstrap results should the SSM/I sensor cease to operate. The close match between the ABA and SBA results is encouraging, as it bodes well for future efforts to extend climate records despite the necessity of instrument changes, as no instrument can last forever.

[27] Interesting as ice concentrations and extents might be, trends in the variables are of considerably more interest for climate change studies. Although the AMSR-E data record is far too short for establishing climate trends, the record does allow calculation of a 4.5-year linear least squares fit and comparison between the short-term trend values (calculated as the slopes of the least squares fit lines) from the two algorithms. The July 2002 to December 2006 ice extent trends calculated from monthly anomalies are $-65{,}000 \pm 46{,}000$ km^2/a using the ABA algorithm and $-67{,}000 \pm 45{,}000$ km^2/a using the NT2 algorithm, refreshingly within 5% of each other and interestingly negative. In studies examining a much longer record, the Southern Ocean was found to have increasing ice extents, overall, from the late 1970s to the mid-1990s and the late 1990s, with, for example, *Zwally et al.* [2002] finding an ice extent trend of $+11{,}000 \pm 4{,}000$ km^2/a for the period 1979–1998 and *Stammerjohn and Smith* [1997] earlier finding comparable results for 1978–1995. The increase in Southern Ocean ice found by Zwally et al., Stammerjohn and Smith, and others is in marked contrast to the decreases in Arctic sea ice coverage since the late 1970s, determined, for instance, by *Parkinson et al.* [1999] for 1978–1996 annual and seasonal results, by *Stroeve et al.* [2005] for 1979–2004 late summer results, by *Comiso* [2006] for 1979–2006 winter results, and by *Meier et al.* [2007] for 1979–2006 annual and monthly results. This hemispheric contrast has garnered the attention of the Intergovernmental Panel on Climate Change [e.g., *Houghton et al.*, 2001] as well as many others. The sea ice covers of both hemispheres experience considerable interannual variability, and hence the decreases in the ice cover of the Southern Ocean over the period 2002–2006 (Figure 9) might simply reflect more interannual variability. Still, it is interesting that the Southern Ocean, which had been experiencing increasing ice extents, has for the short 2002–2006 period experienced some marked ice extent decreases.

[28] **Acknowledgments.** Nick DiGirolamo and Rob Gersten are thanked for their considerable help in the generation of the figures, and the Cryospheric Sciences Program at NASA Headquarters is thanked for funding the work.

References

Bjorgo, E., O. M. Johannessen, and M. W. Miles (1997), Analysis of merged SMMR-SSMI time series of Arctic and Antarctic sea ice parameters 1978–1995, *Geophys. Res. Lett.*, *24*(4), 413–416.

Bromwich, D. H., and D. D. Kurtz (1984), Katabatic wind forcing of the Terra Nova Bay polynya, *J. Geophys. Res.*, *89*(C3), 3561–3572.

Cavalieri, D. J., P. Gloersen, and W. J. Campbell (1984), Determination of sea ice parameters with the Nimbus 7 SMMR, *J. Geophys. Res.*, *89*(D4), 5355–5369.

Cavalieri, D. J., C. L. Parkinson, P. Gloersen, J. C. Comiso, and H. J. Zwally (1999), Deriving long-term time series of sea ice cover from satellite passive-microwave multisensor data sets, *J. Geophys. Res.*, *104*(C7), 15,803–15,814.

Comiso, J. C. (2006), Abrupt decline in the Arctic winter sea ice cover, *Geophys. Res. Lett.*, *33*, L18504, doi:10.1029/2006GL027341.

Comiso, J. C., and C. L. Parkinson (2008), Arctic sea ice parameters from AMSR-E data using two techniques and comparisons with sea ice from the Special Sensor Microwave Imager (SSM/I), *J. Geophys. Res.*, doi:10.1029/2007JC004255, in press.

Comiso, J. C., T. C. Grenfell, D. L. Bell, M. A. Lange, and S. F. Ackley (1989), Passive microwave in situ observations of winter Weddell sea ice, *J. Geophys. Res.*, *94*(C8), 10,891–10,905.

Comiso, J. C., D. J. Cavalieri, C. L. Parkinson, and P. Gloersen (1997), Passive microwave algorithms for sea ice concentration: A comparison of two techniques, *Remote Sens. Environ.*, *60*(3), 357–384.

Comiso, J. C., D. J. Cavalieri, and T. Markus (2003), Sea ice concentration, ice temperature, and snow depth using AMSR-E data, *IEEE Trans. Geosci. Remote Sens.*, *41*(2), 243–252.

Gloersen, P., W. J. Campbell, D. J. Cavalieri, J. C. Comiso, C. L. Parkinson, and H. J. Zwally (1992), Arctic and Antarctic sea ice, 1978–1987: Satellite passive-microwave observations and analysis, *NASA Spec. Publ.*, *SP-511*, 290 pp.

Houghton, J. T., Y. Ding, D. J. Griggs, M. Noguer, P. J. van der Linden, X. Dai, K. Maskell, and C. A. Johnson (Eds.) (2001), *Climate Change 2001: The Scientific Basis: Contribution of Working Group 1 to the Third Assessment Report of the Intergovernmental Panel on Climate Change*, 881 pp., Cambridge Univ. Press, New York.

Kawanishi, T., T. Sezai, Y. Ito, K. Imaoka, T. Takeshima, Y. Ishido, A. Shibata, M. Miura, H. Inahata, and R. W. Spencer (2003), The Advanced Microwave Scanning Radiometer for the Earth Observing System (AMSR-E), NASDA's contribution to the EOS for global energy and water cycle studies, *IEEE Trans. Geosci. Remote Sens.*, *41*(2), 184–194.

Markus, T., and D. J. Cavalieri (2000), An enhancement of the NASA team sea ice algorithm, *IEEE Trans. Geosci. Remote Sens.*, *38*(3), 1387–1398.

Markus, T., C. Kottmeier, and E. Fahrbach (1998), Ice formation in coastal polynyas in the Weddell Sea and their impact on oceanic salinity, in *Antarctic Sea Ice: Physical Processes, Interactions and Variability*, *Antarct. Res. Ser.*, vol. 74, edited by M. O. Jeffries, pp. 273–292, AGU, Washington, D. C.

Meier, W. N., J. Stroeve, and F. Fetterer (2007), Whither Arctic sea ice? A clear signal of decline regionally, seasonally and extending beyond the satellite record, *Ann. Glaciol.*, *46*, 428–434.

Olbers, D., D. Borowski, C. Volker, and J.-O. Wolff (2004), The dynamical balance, transport and circulation of the Antarctic Circumpolar Current, *Antarct. Sci.*, *16*(4), 439–470.

Parkinson, C. L. (2003), Aqua: An Earth-observing satellite mission to examine water and other climate variables, *IEEE Trans. Geosci. Remote Sens.*, *41*(2), 173–183.

Parkinson, C. L. (2004), Southern Ocean sea ice and its wider linkages: Insights revealed from models and observations, *Antarct. Sci.*, *16*(4), 387–400.

Parkinson, C. L., D. J. Cavalieri, P. Gloersen, H. J. Zwally, and J. C. Comiso (1999), Arctic sea ice extents, areas, and trends, 1978–1996, *J. Geophys. Res.*, *104*(C9), 20,837–20,856.

Stammerjohn, S. E., and R. C. Smith (1997), Opposing Southern Ocean climate patterns as revealed by trends in regional sea ice coverage, *Clim. Change*, *37*(4), 617–639.

Stroeve, J. C., M. C. Serreze, F. Fetterer, T. Arbetter, W. Meier, J. Maslanik, and K. Knowles (2005), Tracking the Arctic's shrinking ice cover: Another extreme September minimum in 2004, *Geophys. Res. Lett.*, *32*, L04501, doi:10.1029/2004GL021810.

Zwally, H. J., J. C. Comiso, C. L. Parkinson, D. J. Cavalieri, and P. Gloersen (2002), Variability of Antarctic sea ice 1979–1998, *J. Geophys. Res.*, *107*(C5), 3041, doi:10.1029/2000JC000733.

J. C. Comiso and C. L. Parkinson, Cryospheric Sciences Branch, NASA Goddard Space Flight Center, Code 614.1, Greenbelt, MD 20771, USA. (claire.l.parkinson@nasa.gov)